Mem. S.A.It. Vol. 91, 332

Memorie della

Star formation rate in simulated clusters

E. Rasia[1], L. Bassini[1,2], M. Valentini[1,3], V. Biffi[1,3], S. Borgani[1,2], K. Dolag[3], G. L. Granato[1], G. Murante[1], A. Ragagnin[1], C. Ragone-Figueroa[1,4], G. Taffoni[1], and L. Tornatore[1]

[1] INAF – Astronomical Observatory of Trieste, via Tiepolo 11, I-34143 Trieste, Italy
e-mail: elena.rasia@inaf.it
[2] Astronomy Unit-Dep. of Physics, University of Trieste, via Tiepolo 11, 34143, Trieste, Italy
[3] Universitäts-Sternwarte München, Fakultät für Physik, LMU Munich, Scheinerstr. 1, 81679 München, Germany
[4] IATE, CONICET, Universidad Nacional de Córdoba, Laprida 854, X5000BGR, Córdoba, Argentina

Abstract. The star formation rate (SFR) of simulated galaxy clusters is compared to recent observational studies at $z = 0$ and $z \sim 2$. In particular, we analyze a set of zoom-in cosmological hydrodynamical simulations centered on twelve clusters and carried out with the GADGET-3 TreePM/SPH code. We find that simulated central galaxies produce an excess of stars at $z = 0$, however at $z \sim 2$ simulations under-predict the normalization of the relation SFR–stellar mass of star forming galaxies by a factor of about 3 and are unable to reproduce the observed starburst population. We conclude that the adopted sub-grid model for star formation (Springel & Hernquist 2003), introduced to reproduce the self-regulated evolution of quiescent galaxies, is not suitable to describe violent events like high-redshift starbursts, independently of the choice of the parameters for the star formation and active-galactic-nuclei models. A more extensive analysis is present in Bassini et al. (2020).

Key words. Galaxies: clusters: general Galaxies: star formation Galaxies: starburst method: numerical Hydrodynamics

1. Introduction

Numerical simulations have been unable to reproduce the high star formation rates (SFR) observed in proto-clusters characterized by over-densities of dusty star-forming galaxies (Granato et al. 2015). This result adds to a long standing difficulty for cosmological simulations to reproduce star formation properties of galaxies at high redshift, one of them being the main sequence of star forming galaxies (i.e., the relation between the SFR and the galaxy stellar mass), computed at the maximum of the cosmic SFR density (Davé et al. 2019). Indeed, Granato et al. (2015) found that the bulk of star formation within the observed putative progenitors of massive galaxy clusters occurred at higher rates and lasted less than in simulations. This conclusion was based on the observations available five years ago, characterized by low angular resolution and for which the SFRs were evaluated over one to a few Mpc scale. More recently, with instruments like ALMA, it has been possible to resolve single sources within protoclusters (Wang et al. 2018,

Gómez-Guijarro et al. 2019). At the same time, progress has been made to increase the numerical resolution needed to resolve higher density peaks and related higher SFRs. Thanks to the CINECA allocated time we were able to carry out a sample of simulations at a resolution 10 times better than what previous analyzed (Section 2) and one region at a resolution improved by 250 times (Section 4).

2. Simulation

The analysis presented in this report is based on a set of 12 hydrodynamical zoom-in simulations evolved in a ΛCDM cosmology, with parameters: $\Omega_m = 0.24$, $\Omega_b = 0.037$, $n_s = 0.96$, $\sigma_8 = 0.8$, and $H_0 = 100\ h$ km s^{-1} = 72 km s^{-1} Mpc^{-1}. The regions are extracted from a parent dark-matter (DM) only simulation of $1h^{-1}$ Gpc side, resimulated at higher resolution (with $m_{\rm DM} = 8.4 \times 10^7 h^{-1}{\rm M}_\odot$ for DM and $m_{\rm gas} = 1.6 \times 10^7 h^{-1}{\rm M}_\odot$ for the initial gas particles) and with the addition of baryonic physics. The simulations are carried out with the code GADGET-3, a modified version of the Tree-PM Smoothed-Particle Hydrodynamics public code GADGET2 (Springel 2005). An extensive description of the code (including relevant references) is presented in Bassini et al (2020) along with the details of the sub-grid models adopted for the unresolved baryonic physics (such as the prescription of metal-dependent radiative cooling; the model of star formation and associated feedback; the metal enrichment and chemical evolution; the stellar yields; the active-galactic-nuclei (AGN) feedback). The Plummer equivalent gravitational softening adopted for DM particles is $4.2h^{-1}$ kpc (comoving) at $z > 2$ and $1.4h^{-1}$ kpc (physical) otherwise. The softening lengths for gas, star, and blackholes particles are 1.4, 0.35, and $0.35h^{-1}$ kpc, respectively.

3. Results

3.1. SFR at $z = 0$

We verified that the stellar mass of the simulated galaxies (within either 30 or 50 kpc) reproduce well the galaxy mass function derived by Bernardi et al. (2013) and corrected as in Bassini et al. (2020). On the other hand, our simulated brightest cluster galaxies (BCG) tend to be twice as massive as those observed in similar mass cluster by Kravtsov et al. (2018) and De Maio et al. (2018). After some tests, we conclude that the current modelling of the sub-grid physics, especially the AGN feedback, rather than the numerical resolution, impedes us to simultaneously recover the galaxy mass function and the BCG stellar mass. On top of larger masses, the simulated BCGs also over-produce stars at recent times with respect to observations (Fig.1 left) and to a higher star formation efficiency as confirmed by the comparison of the specific SFR defined as the SFR normalized by the BCG stellar mass (Fig.1 right).

3.2. SFR at higher redshift ($z > 2$)

The inequality between simulated and observed SFR changes sign at higher redshifts. The left panel of Fig. 2 refers to $z \sim 2.3$, around the peak of the cosmic SFR, when we detect the maximum discrepancy. The average observed main-sequence behavior (red lines) is at the highest end of the distribution of simulated galaxies whose mean trend is a factor of 3 below the observed one. Furthermore, simulations cannot reproduce any existing observed objects (blue and green points) characterized by extreme values of SFR (see also Granato et al. 2015). More generally, the observations suggest that the SFRs are distributed as a double Gaussian around the main sequence (Sargent et al. 2012) while simulations fail to obtain any hint of a second Gaussian associated to the starburst galaxies (Fig.2 right panel). Interestingly, the gap between observations and simulations subsists also for simulations obtained from cosmological volumes (such as Magneticum shown in the right panel of Fig. 2).

3.3. Global SFR

Lastly, in Fig.3 we show the comparison of the evolution of the ratio between the global SFRs, computed by summing over all cluster galax-

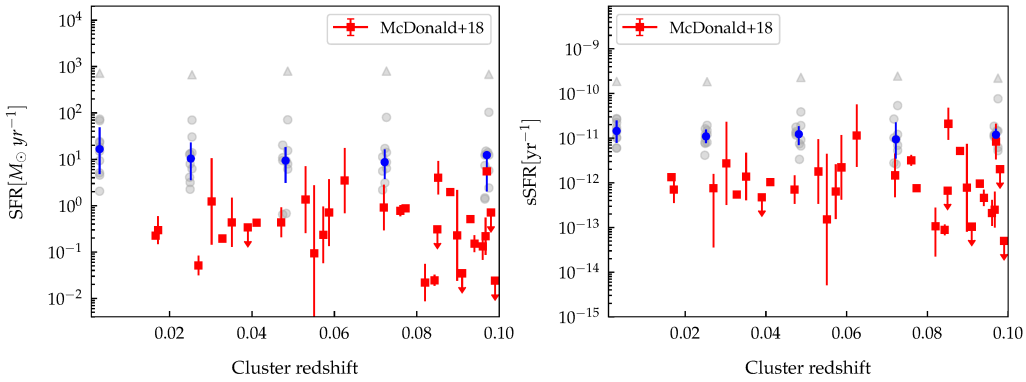

Fig. 1. BCG SFR (left panel) and specific SRF (right panel) in simulations (grey points) and in the observations from McDonald et al. 2018 (red points). Measures are done within 30 pkpc in 2D. The slight offset of the grey point is for visualization only. Median, 16th, and 84th percentiles are shown in blue.

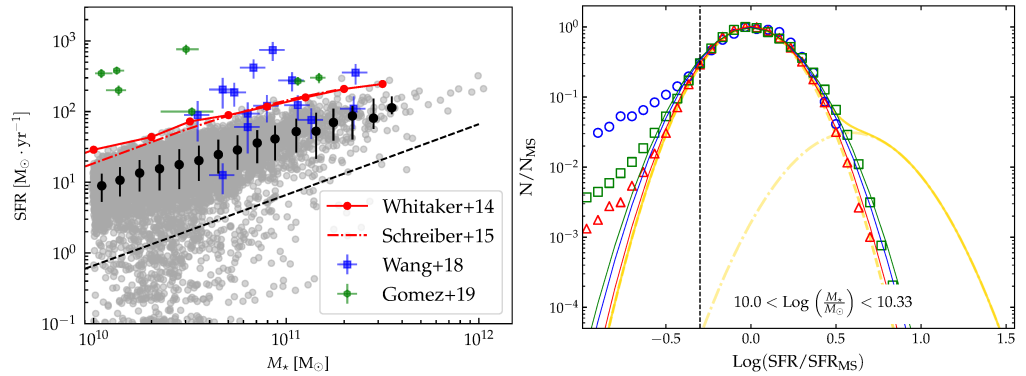

Fig. 2. Left panel: SFR as a function of galaxy stellar mass at $z \sim 2.3$. Red lines and green and blue points are observational data. Grey points are galaxies in our simulations considering a 3D aperture of 30 kpc. Black points and error are median and percentiles as in Fig.1. Right Panel: SFR distribution around the main sequence of simulated clusters from our sample (blue), the Magneticum simulations (red and green) and observations (yellow, Sargent et al. 2012).

ies, and the cluster mass. The simulated curve grows with redshift as seen in observations but the rate is shallower. In conclusion, simulations overestimate also the global SFRs at low redshift and underestimate those at high redshifts (see also Ragone-Figueroa et al. 2018).

4. Discussion and conclusions

The fraction of starburst galaxies and the normalization of the main sequence might depend on the choices of the parameters of the sub-grid model. We therefore resimulate one region six different times and each time we vary the following conditions:

(i) timescale for star formation;
(ii) density threshold for star formation;
(iii) both timescale and density threshold;
(iv) supernovae thermal feedback;
(v) AGN model;
(vi) turning off the AGN feedback.

Despite all these versions produce a different amount of cold gas and star formation efficiencies, which lead to various galaxy mass distributions, the normalization of the overall main

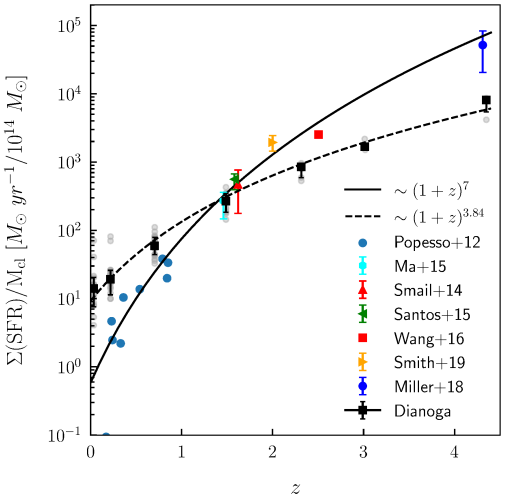

Fig. 3. SFR normalised by cluster mass as a function of redshift. Black squares represent median values from Dianoga simulations (grey points). Dashed black line is the best fit to simulations. Coloured points are observational data. The solid black line shows an empirical fit to data suggested by Cowie et al. (2004) and Geach et al. (2006).

sequence and the absence of starburst galaxies are independent from the considered variation. Finally, two simulations were run at 25 times better resolution with two values of the depletion timescale and the results shown before were confirmed. However, when a small group ($M = 10^{13}$ $M_\odot$) was run at this high resolution with MUPPI-AGN as sub-grid model (Valentini et al. 2020) instead of the effective model of Springel & Hernquist (2003), the high-redshift star formation burst seemed to be reproduced for the highest level of star formation efficiency. This may possibly point to the effective model not being as sensitive as the MUPPI model to the variation of the star formation efficiency. It may also suggest how important it is to estimate the star formation rate from the molecular phase, rather than from the cold gas. This speculation will be further investigated in the near future with simulations run with an ISCRA-B allotted time.

Acknowledgements. We would like to thank Volker Springel for making the GADGET-3 code available to us. This project has received funding from: Horizon 2020 grant agreement No 671553 and No 754337; Excellence Cluster ORIGINS EXC-2094 - 390783311;ASI-INAF n.2017-14-H.0; CONICET; SeCyT; Horizon 2020-Marie Sklodowska-Curie grant agreement No 734374, PRIN-MIUR 2015W7KAWC, the INFN INDARK grant. Simulations have been carried out using MARCONI at CINECA (Italy); MENDIETA Cluster from CCAD-UNC, which is part of SNCAD-MinCyT (Argentina); the Tianhe-2 platform of the Guangzhou Supercomputer Center (2017YFB0203300). The post-processing has been performed using the PICO HPC cluster at CINECA through our expression of interest. We acknowledge the computing centre of Cineca and INAF, under the coordination of the "Accordo Quadro MoU per lo svolgimento di attività congiunta di ricerca Nuove frontiere in Astrofisica: HPC e Data Exploration di nuova generazione", for the availability of computing resources and support.

References

Bassini, L., et al. 2020, A&A, 642, A37
Bernardi, M., et al. 2013, MNRAS, 436, 697
Biffi, V., et al. 2017, MNRAS, 468, 531
Cowie, L. L., et al. 2004, ApJ, 603, L69
Davé, R., et al. 2019, MNRAS, 486, 2827
DeMaio, T., et al. 2018, MNRAS, 474, 3009
Geach, J. E., et al. 2006, ApJ, 649, 661
Goméz-Guijarro, C., et al. 2019, ApJ, 872, 117
Granato, G. L., et al. 2015, MNRAS, 450, 1320
Kravtsov, A., et al. 2018, Astr. Lett., 44, 8
Ma, C. J., et al. 2015, ApJ, 806, 257
McDonald, M., et al. 2018, ApJ, 858, 45
Miller, T. B., et al. 2018, Nature, 556, 469
Popesso, P., et al. 2012, A&A, 537, A58
Ragone-Figueroa, C., et al. 2013, MNRAS, 436, 1750
Ragone-Figueroa, C., et al. 2018, MNRAS, 479, 1125
Santos, J. S., et al. 2015, MNRAS, 447, L65
Sargent, M. T., et al. 2012, ApJ, 747, L31
Schreiber, C., et al. 2015, A&A, 575, A74
Smail, I., et al. 2014, ApJ, 782, 19
Smith,C.M., et al., 2019, MNRAS, 486, 4304
Springel, V., 2005, MNRAS, 364, 1105
Springel, V. & Hernquist, L. 2003, MNRAS, 339, 289
Valentini, M., et al. 2020, MNRAS, 491, 2779
Wang, T., et al. 2016, ApJ, 828, 56
Wang, T., et al. 2018, ApJ, 867, L29
Whitaker, K. E., et al. 2014, ApJ, 795, 104